Pergamon

*Int. J. Heat Mass Transfer.* Vol. 40, No. 10, pp. 2419–2430, 1997
© 1997 Elsevier Science Ltd
Printed in Great Britain. All rights reserved
0017–9310/97 $17.00+0.00

PII: S0017–9310(96)00271–2

# Buoyant instabilities in downward flow in a symmetrically heated vertical channel

G. EVANS

Thermal and Plasma Processes Department, Sandia National Laboratories, Livermore, CA 94550, U.S.A

and

R. GREIF

Mechanical Engineering Department, University of California, Berkeley, CA 94720, U.S.A

(*Received* 16 *February* 1996 *and in final form* 15 *July* 1996)

**Abstract**—This study of the downward flow of nitrogen in a tall, partially heated vertical channel (upstream isothermal at $T_{in}^*$, heated region isothermal at $T_s^*$, downstream adiabatic) shows the strong effects of buoyancy even for small temperature differences. Time-dependent oscillations including periodic flow reversals occur along the channel walls. Although the flow and heat transfer are asymmetric, the temperature and axial component of velocity show symmetric reflections at two times that are half a period apart and the lateral component of velocity shows antisymmetric reflections at the two times. There is strong interaction between the downward flow in the central region of the channel and the upward flow along the heated channel walls. At the top of the heated region, the upward buoyant flow turns toward the center of the channel and is incorporated into the downward flow. Along the channel centerline there are nonmonotonic variations of the axial component of velocity and temperature and a large lateral component of velocity that reverses direction periodically. Results are presented for $Re = 219.7$ and $Gr/Re^2 = 1.83$, 8.0 and 13.7. The heat transfer and the frequency of the oscillations increase and the flow and temperature fields become more complex as $Gr/Re^2$ increases. The results have applications to fiber drying, food processing, crystal growth, solar energy collection, cooling of electronic circuits, ventilation, etc. © 1997 Elsevier Science Ltd. All rights reserved.

## INTRODUCTION

Buoyant effects in fluid flow in vertical tubes or channels are common and have been studied extensively (Ostrach [1]; Morton [2]; Scheele and Hanratty [3]; Lawrence and Chato [4]; Zeldin and Schmidt [5]; Quintiere and Mueller [6]; Cebeci *et al.* [7]; Yao [8]; Shadday [9]; Habchi and Acharya [10]; Wang *et al.* [11]). Recently, time-dependent and asymmetric opposed mixed convection flow in a vertical channel with specified heat flux conditions has been studied numerically for low $Pr$ (Chang and Lin [12]) and for $Pr = 0.72$ and 7.0 (Lin *et al.* [13]). Other studies concerning the unstable nature of opposed flow mixed convection have been made by Guerrero and Hart [14]; Rogers and Yao [15]; Joye and Jacobs [16]; and Gau *et al.* [17].

In [15], nonlinear instability analysis was used to predict flow instability in both aiding and opposing mixed convection in a vertical tube with a linearly varying wall temperature profile. For aiding flow the heat transfer predicted from the single wave theory is smaller than what is observed; for $Re = 600$, the predicted heat transfer is increased by considering multiple waves. In Ref. [16], periodic temperature oscillations in opposed flow mixed convection in water in a partially heated (isothermal) vertical tube were measured upstream of the start of the heated region for $Re = 600$ and $Gr = 5 \times 10^7$; the heat transfer was shown to lie along a forced asymptote for $Re < 2000$. In Ref. [17], temperature fluctuations and unstable flow of air were observed in opposed flow mixed convection in a vertical heated converging channel (one wall constant heat flux, the other insulated) for $Gr/Re^2 = 40$ (where $Gr$ is based on the heat flux) and $Re = 250$; for a parallel plate channel the heat transfer was correlated with two different expressions depending on the range of $Gr/Re^2$.

In Lin *et al.* [13], the cold downward forced flow first passed through an insulated region before entering the constant heat flux region; time variations of the average heat transfer, the axial component of velocity, and the temperature at two axial locations in the middle and at the downstream ends of the constant heat flux region were presented for $Gr/Re^2$ up to 4. In some applications a cold section is located above the heated region. The effects of different thermal boundary conditions above the heated region are important since strong buoyancy causes the fluid flow to move upward along the heated surface. This effect is more

## NOMENCLATURE

| | |
|---|---|
| $Gr$ | Grashof number, $g(T_s^*-T_{in}^*)w^{*3}/(T_{in}^* \nu_{in}^{*2})$ |
| $Gr/Re^2$ | mixed convection parameter, $g(T_s^*-T_{in}^*)w^*/(T_{in}^* u_{in}^{*2})$ |
| $L$ | dimensionless length of heated region, $L = L^*/w^* = 8.6$ |
| $Nu$ | local Nusselt numbers, $-k\,\partial T/\partial y\|_{y=0}$, $k\,\partial T/\partial y\|_{y=1}$ |
| $Nu_{avg}$ | spatially averaged Nusselt numbers, $1/L\int_0^L Nu\Delta x$ |
| $Pr$ | Prandtl number, $c_{pin}^* \mu_{in}^* / k_{in}^*$ |
| $Re$ | Reynolds number, $\rho_{in}^* \mu_{in}^* w^*/\mu_{in}^*$ |
| $T$ | temperature, $(T^*-T_{in}^*)/(T_s^*-T_{in}^*)$ |
| $c_p$ | specific heat |
| $g$ | acceleration of gravity |
| $k$ | thermal conductivity |
| $p_m$ | motion pressure |
| $t$ | time |
| $u$ | axial component of velocity |
| $u_{in}^*$ | average inlet velocity [cm $s^{-1}$] |
| $v$ | lateral component of velocity |
| $w^*$ | channel width [cm] |
| $x$ | axial coordinate |
| $y$ | lateral coordinate. |

Greek symbols

| | |
|---|---|
| $\rho$ | density |
| $\mu$ | dynamic viscosity |
| $\nu$ | kinematic viscosity. |

Subscripts and superscripts

| | |
|---|---|
| in | evaluated at channel inlet |
| s | at channel surfaces |
| * | dimensional quantity. |

pronounced at strong buoyancy as shown in this study.

The results for the axial and lateral profiles of both velocity components and temperature and axial profiles of the heat transfer show the asymmetric nature of the phenomena as well as symmetric reflections at times that are half a period apart. The results exhibit nonmonotonic variations of the axial component of velocity and temperature and a large lateral component of velocity along the channel centerline. These effects can occur in practice for small temperature differences. The results have applications to fiber drying, food processing, crystal growth, solar energy collection, electronic circuit cooling, ventilation, etc. For example, in fiber drying, the opposed flow instabilities give rise to low frequency oscillations which can lead to lateral fiber motion and fiber tangling and breakage.

## ANALYSIS

The geometry of the system is shown in Fig. 1. Nitrogen at atmospheric pressure and 300 K flows downward in a vertical channel with walls maintained at 300 K for $x < 0$. At $x = 0$ the downward flow encounters a second region of the channel ($0 \leqslant x < 8.6$) that is at an elevated temperature, $T_s^*$. Beyond the second region ($x \geqslant 8.6$) the gas flows through a final region of the channel that is adiabatic. The problem is symmetric about the centerline of the channel ($y = 0.5$). At the inlet ($x = -4.3$), the velocity distribution is parabolic. The section above the heated (isothermal at $T_s^*$) region serves two purposes: first, it allows the inlet boundary conditions to be applied where the flow is unidirectional, and second, the effects of a cold surface above a hot zone on the rising, heated buoyant flow can be determined. In the

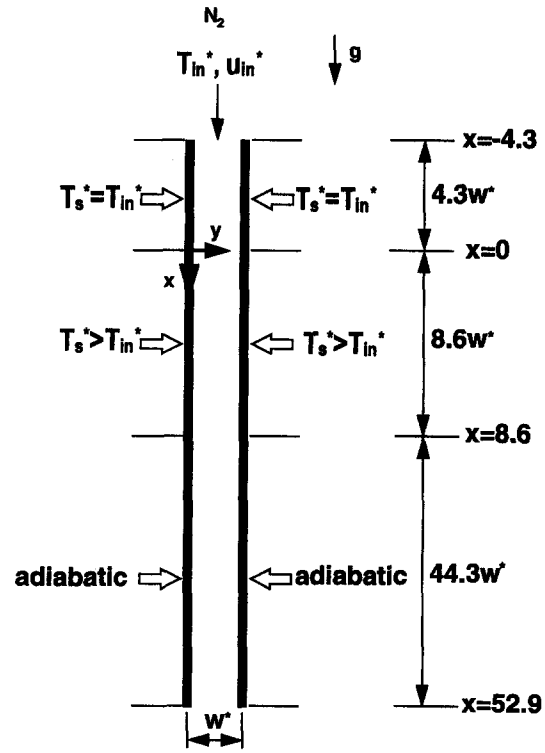


Fig. 1. Geometry (not to scale) and boundary conditions.

adiabatic region below the heated region, the flow returns to the unidirectional condition before exiting the channel. The two-dimensional, planar, dimensionless equations for the flow of a single component gas at low Mach number are:

$$\frac{\partial \rho}{\partial t} + \frac{\partial(\rho u)}{\partial x} + \frac{\partial(\rho v)}{\partial y} = 0 \qquad (1)$$

$$\frac{\partial(\rho u)}{\partial t}+\frac{\partial}{\partial x}\left(\rho uu-\frac{\mu}{Re}\frac{\partial u}{\partial x}\right)+\frac{\partial}{\partial y}\left(\rho vu-\frac{\mu}{Re}\frac{\partial u}{\partial y}\right)$$
$$=-\frac{\partial p_m}{\partial x}-\frac{Gr}{Re^2}\frac{T}{[1+T(T_s^*/T_{in}^*-1)]}$$
$$+\frac{1}{Re}\frac{\partial}{\partial x}\left[\mu\frac{\partial u}{\partial x}-\frac{2\mu}{3}\left(\frac{\partial u}{\partial x}+\frac{\partial v}{\partial y}\right)\right]+\frac{1}{Re}\frac{\partial}{\partial y}\left(\mu\frac{\partial v}{\partial x}\right) \quad (2)$$

$$\frac{\partial(\rho v)}{\partial t}+\frac{\partial}{\partial x}\left(\rho uv-\frac{\mu}{Re}\frac{\partial v}{\partial x}\right)+\frac{\partial}{\partial y}\left(\rho vv-\frac{\mu}{Re}\frac{\partial v}{\partial y}\right)$$
$$=-\frac{\partial p_m}{\partial y}+\frac{1}{Re}\frac{\partial}{\partial y}\left[\mu\frac{\partial v}{\partial y}-\frac{2\mu}{3}\left(\frac{\partial u}{\partial x}+\frac{\partial v}{\partial y}\right)\right]$$
$$+\frac{1}{Re}\frac{\partial}{\partial x}\left(\mu\frac{\partial u}{\partial y}\right) \quad (3)$$

$$\frac{\partial(\rho T)}{\partial t}+\frac{\partial}{\partial x}\left(\rho uT-\frac{1}{Re\cdot Pr}\frac{k}{c_p}\frac{\partial T}{\partial x}\right)$$
$$+\frac{\partial}{\partial y}\left(\rho vT-\frac{1}{Re\cdot Pr}\frac{k}{c_p}\frac{\partial T}{\partial y}\right)$$
$$=\frac{1}{Re\cdot Pr}\frac{k}{c_p^2}\left(\frac{\partial T}{\partial x}\frac{\partial c_p}{\partial x}+\frac{\partial T}{\partial y}\frac{\partial c_p}{\partial y}\right). \quad (4)$$

The gas density is determined from the ideal gas equation of state. The properties of $N_2$ are determined from kinetic theory expressions through the CHEMKIN computer code (Kee *et al.* [18, 19]). Equations (1)–(4) are for variable property flow and heat transfer; however, the cases presented in this work are for small temperature differences (maximum 15 K), and the effect of variable properties is primarily in the density changes in the gravitational term (2nd term on the right-hand-side in equation (2)). Reference quantities for nondimensionalization are: channel width, $w^*$; average inlet flow velocity $u_{avg}^*$; temperature difference $(T_s^*-T_{in}^*)$, where $T=(T^*-T_{in}^*)/(T_s^*-T_{in}^*)$; and properties evaluated at the inlet temperature, $T_{in}^*$. The dimensionless parameters in the above equations are the Grashof number $Gr=g(T_s^*-T_{in}^*)w^{*3}/(T_{in}^*\nu_{in}^{*2})$, the Reynolds number $Re=u_{in}^*w^*/\nu_{in}^*$, and the Prandtl number $Pr=c_{pin}^*\mu_{in}^*/k_{in}^*$.

The boundary conditions are (for $t>0$):

at $x=-4.3$, for $0\leqslant y\leqslant 1$:
$$T=0,\quad u=6y(1-y),\quad v=0;$$
at $y=0$ and 1, for $-4.3\leqslant x<0$:
$$T=0,\quad u=0,\quad v=0;$$
at $y=0$ and 1, for $0\leqslant x<8.6$;
$$T=1,\quad u=0,\quad v=0;$$
at $y=0$ and 1, for $8.6\leqslant x\leqslant 52.9$:
$$\partial T/\partial y=0,\quad u=0,\quad v=0;$$
at $x=52.9$, for $0\leqslant y\leqslant 1$:
$$\partial T/\partial x=\partial u/\partial x=\partial v/\partial x=0.$$

The initial conditions are:

at $t=0$, for $0\leqslant y\leqslant 1$ and for $-4.3\leqslant x\leqslant 52.9$: $T=0$, $u=6y(1-y)$, $v=0$.

*Numerical solution*

The conservation equations (1)–(4) were integrated over control volumes and discretized using the hybrid differencing scheme (Patankar [20]). The continuity equation was used in the SIMPLER method to determine the pressure, $p_m$. The time derivatives were discretized using the backward Euler method. A sequential line by line relaxation iterative method was applied to solve the discretized equations and boundary conditions. The results shown here were determined using 205 $x$ grids and 34 $y$ grids, with 50 $x$ grids in the heated zone. The grid spacing was nonuniform and finer near the surface and the start of the heated region (at $x=0$). The time step was uniform ($\Delta t=0.0357$) for all the results shown.

*Convergence criteria*

An iterative method was used to solve the coupled, nonlinear set of equations at each time step. Underrelaxation factors (typical values were 0.05–0.5) were used for the momentum and energy conservation equations to avoid numerical instabilities; no underrelaxation was applied to the pressure and the pressure correction equations. The convergence criteria were set as follows: iterations within a time step were continued until the relative changes of all variables at all control volumes from one iteration to the next were less than $10^{-4}$ or until a preset maximum number of iterations (typically 200–300) had occurred. For $Gr/Re^2=1.83$, after the initial transient disturbances (which lasted until $t\geqslant 100$, approximately) subsided, about 60–70 iterations were required per time step. Global mass balances in the channel were satisfied to better than 1%.

*Grid and time step sensitivities*

The number of grids in the $y$ direction was varied from 26 to 42 and the number of grids in the $x$ direction within the heated region was varied from 38 to 60 for $Gr/Re^2=8$. Significant differences existed between results obtained using a $50\times 26$ $(x,y)$ grid in the heated region compared with results from a $50\times 34$ grid. However, comparing results from a $50\times 42$ grid with the $50\times 34$ grid showed good agreement for all quantities (within 1–3%; a maximum difference of 5% occurred in the peak value of the local Nusselt number). Comparisons made between results computed on $50\times 34$ and $60\times 34$ grids in the heated region

showed good agreement to within 1–5% depending on the quantities compared (magnitude and frequency of the oscillations of velocity, temperature and average and local Nusselt numbers). As a result, the $50 \times 34$ grid in the heated region was used.

The time step, $\Delta t$, was varied from 0.01785 to 0.14286; for $Gr/Re^2 = 1.83$, results of calculations with $\Delta t = 0.07143$ and 0.0357 agreed to better than 1%; however, for $Gr/Re^2 = 8.0$, significant differences were noted for results calculated at these two time steps. A subsequent calculation using $\Delta t = 0.01785$ showed good agreement with the $\Delta t = 0.0357$ results (within 1–3% for all quantities except a maximum difference of 5% in the magnitude of one of the local Nusselt number peak values). For $Gr/Re^2 = 13.7$, the results at $\Delta t = 0.0357$ agreed with those obtained at 0.01785 to within 2–4%. The time step, $\Delta t = 0.0357$, was used for the results discussed below.

## RESULTS

Nitrogen enters a vertical channel at $x_{in} = x^*/w^* = -4.3$ (Fig. 1) and flows downward with an inlet temperature $T^*_{in} = 300$ K ($T = 0$) and an inlet parabolic velocity profile with an average velocity $u^*_{avg} = 5$ cm s$^{-1}$ ($u = 1$) corresponding to $Re = 219.7$. In the region near the inlet (from $x = -4.3$ to $x = 0$) the channel is maintained at the inlet gas temperature (300 K, $T = 0$); from $x = 0$ to $x = 8.6$ the channel temperature is $T^*_s$ ($T_s = 1$); and from $x = 8.6$ to the exit at $x = 52.9$ the channel walls are adiabatic. Figure 2 shows the flow pattern (marker pathline traces for eight time steps) and the temperature field (the lead arrow of the fluid pathline traces corresponds to the time of the temperature field) in the heated region of the channel for $Re = 219.7$ and $Gr/Re^2 = 13.7$; the features shown are characteristic of all three cases discussed later. In the heated zone, the fluid near the wall rises due to buoyancy which opposes the downward flow in the center of the channel. Just upstream of the start of the heated region, the downward flow (white arrows in Fig. 2), which has a parabolic profile at the inlet of the channel, is constricted by the upward buoyant flows near the walls. As the downward flow enters the heated region it accelerates due to the effects of the temperature increase and the upward buoyant flows near the walls. The distance between arrowheads on the pathline traces is directly proportional to the speed of the gas flow. When the upward buoyant flow reaches the top of the heated region and encounters the cooler upper region, it turns toward the centerline and is incorporated into the rapidly moving downward flow in the central core of the channel. This phenomenon occurs periodically and alternately on the two surfaces. The resulting velocity and temperature fields are complex, asymmetric with respect to the centerline of the channel and periodic.

The first case considered is for $T^*_s = 302$ K corresponding to $Gr/Re^2 = 1.83$. The color shaded contours of the temperature and velocity fields are shown in Fig. 3(a–f) and are clearly not symmetric about the centerline of the channel although the problem specified is symmetric. The results are periodic and the fields are shown at $t = 251.8$ and half a period later at $t = 259.3$. The time $t = 251.8$ corresponds to a minimum temperature at the location $x = 3.6$, $y = 0.19$. Although the fields are nonsymmetric, half a period later Fig. 3(a–d) shows there is a symmetric reflection about the centerline of the channel (of this nonsymmetric field). Note that the lateral component of the velocity, $v$, shows an antisymmetric reflection about the centerline (Fig. 3(e, f)).

Figure 4(a–c) shows the periodic nature of the temperature and velocity at two axial locations ($x = 0.7, 3.6$) within the heated zone. The temperature, $T$, and axial component of velocity, $u$, are shown near one of the channel walls at $y = 0.19$; in addition, the lateral velocity component, $v$, is also shown near the channel centerline at $y = 0.47$. The amplitudes of all the oscillations are largest near the central part of the heated zone ($x = 3.6$ curves). The periodic flow also exhibits flow reversals ($u$ positive and negative in Fig. 4(b)); $v$ also takes on positive and negative values (Fig. 4(c)). A power spectral analysis of the oscillations of the velocity and temperature at selected points using 2048 time steps yields a single period of 15 (frequency of 0.07). For symmetric flows $v$ would be zero at the centerline; here there are large oscillations in $v$ near the centerline which disturb the symmetry of the flow. The oscillations can have a deleterious effect on some processes; e.g. fiber drying, reactor cooling, ventilation, food processing, etc.

Lateral profiles of $T$, $u$ and $v$ are shown at two times ($t = 251.8$ and 259.3) for different axial positions in Fig. 5(a–c) (as stated above, the results are not symmetric about the centerline of the channel). Recall that the time $t = 251.8$ corresponds to a minimum temperature at $x = 3.6$, $y = 0.19$. The upward buoyant flow near the wall does not penetrate upstream into the unheated region ($x < 0$) as shown by the parabolic profile for $u$ (Fig. 5(b)). Figure 5(b) shows that the buoyant upflow along the channel walls in the heated zone results in an enhanced maximum value of $u$ ($u_{max} = 2.5$ at $x = 3.6$). Comparisons of curves at the same axial location $x$ having the same symbols at times that are one-half of a period apart show that both $T$ and $u$ are symmetric about the centerline half a period later (Fig. 5(a, b)), whereas $v$ is antisymmetric about the centerline half a period later (Fig. 5(c)).

Axial variations (which complement the lateral variations of Fig. 5) of temperature and velocity close to and equidistant from both side walls of the channel ($y = 0.19$ and 0.81) are shown in Fig. 6(a–c) at $t = 251.8$ and 259.3. Both $T$ and $u$ clearly exhibit two maxima which are also seen in Fig. 3. Comparisons of $T$ and $u$ at $y = 0.19$, $t = 251.8$ and at $y = 0.81$, $t = 259.3$ overlap, showing symmetry about the centerline half a period later; $v$ shows antisymmetry about

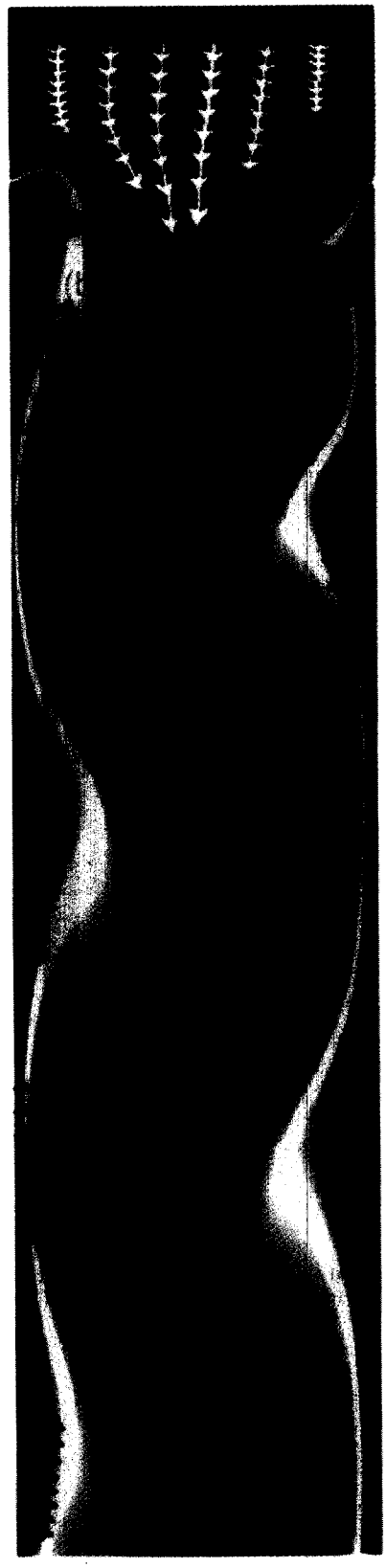

Fig. 2. Temperature field at one instant of time and selected fluid pathlines (markers show the flow patterns over 8 time steps) in the heated region for $Re = 219.7$, $Gr/Re^2 = 13.7$.

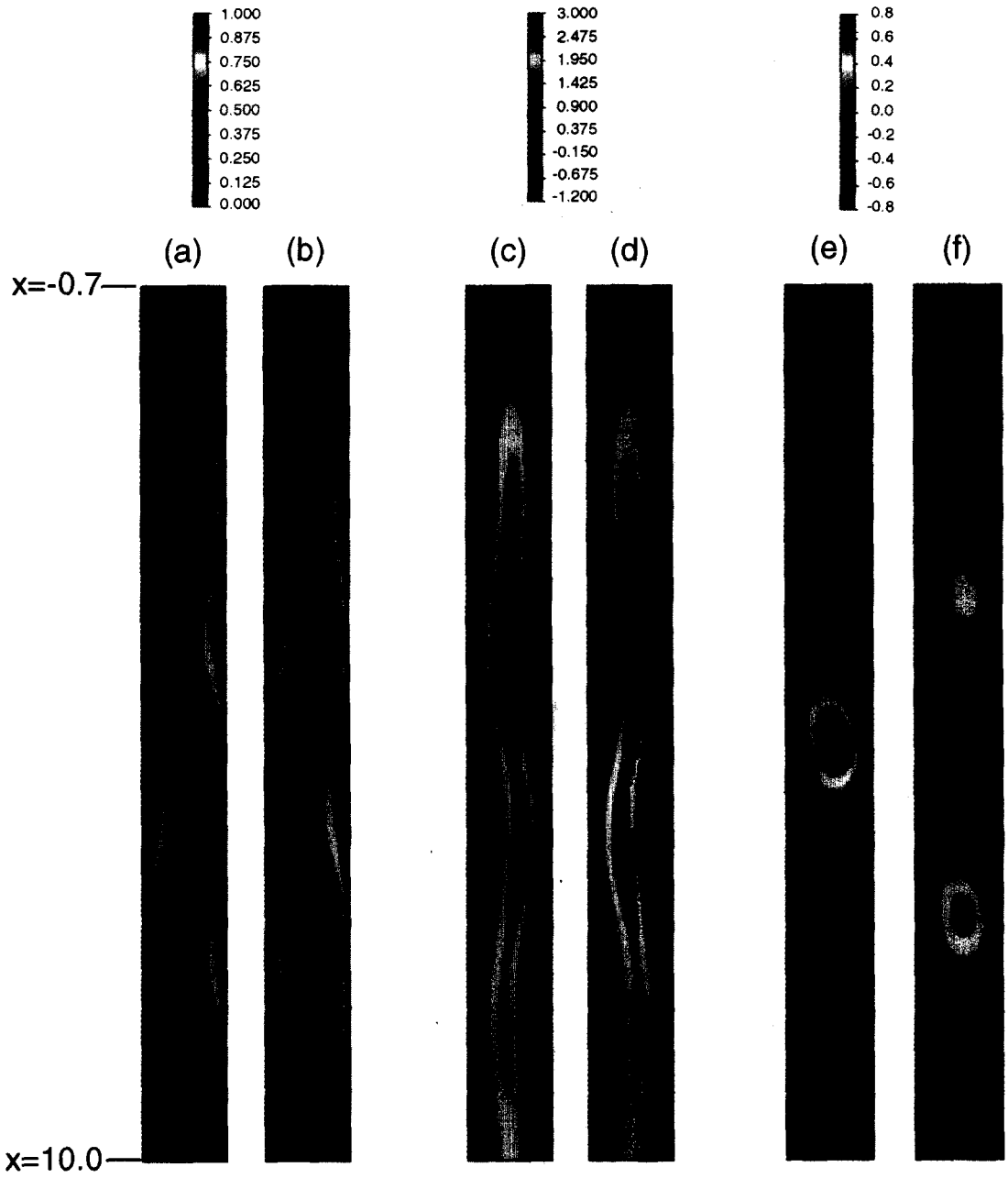


Fig. 3. Temperature and velocity fields at $t = 251.8$ (when $T$ is minimum at $x = 3.6$, $y = 0.19$) [(a), (c), (e)] and half a period later at $t = 259.3$ [(b), (d), (f)]; (a), (b) $T$; (c), (d) $u$; (e), (f) $v$; $Re = 219.7$, $Gr/Re^2 = 1.83$.

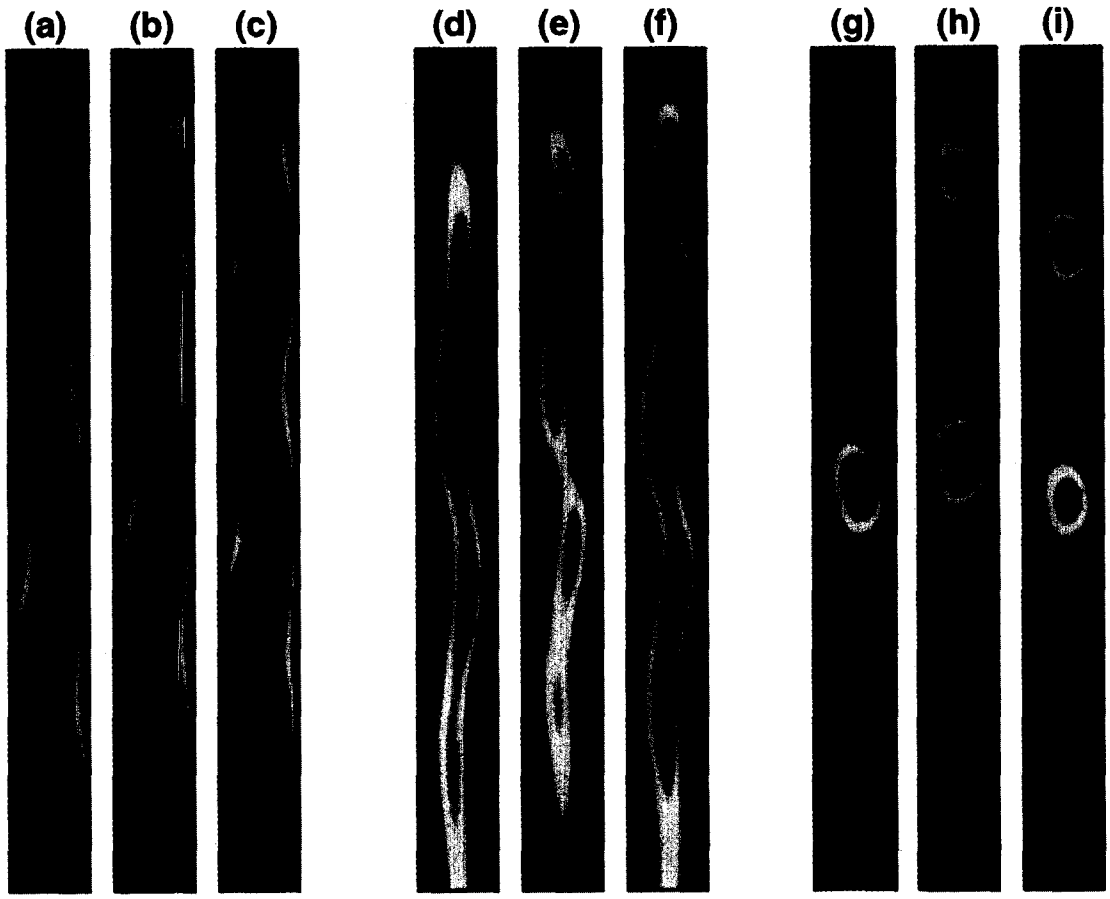


Fig. 9. Temperature and velocity fields at times when $T$ is minimum at $x = 3.6$, $y = 0.19$ for $Re = 219.7$ and three values of $Gr$; (a), (d), (g) : $Gr/Re^2 = 1.83$; (b), (e), (h) : $Gr/Re^2 = 8.0$; (c), (f), (i) : $Gr/Re^2 = 13.7$; (a)–(c) : $T$; (d)–(f) : $u$; (g)–(i) : $v$.

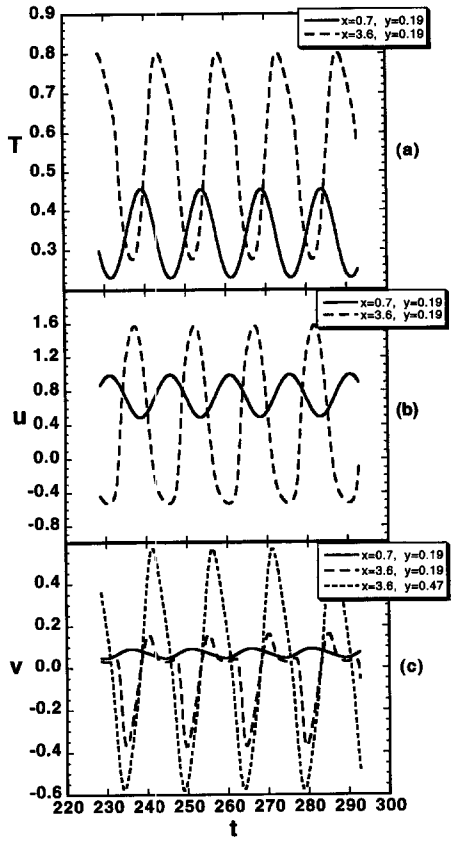


Fig. 4. Time variations of temperature (a) and velocity (b, c) at $y = 0.19$, 0.47 and $x = 0.7$, 3.6; $Re = 219.7$; $Gr/Re^2 = 1.83$.

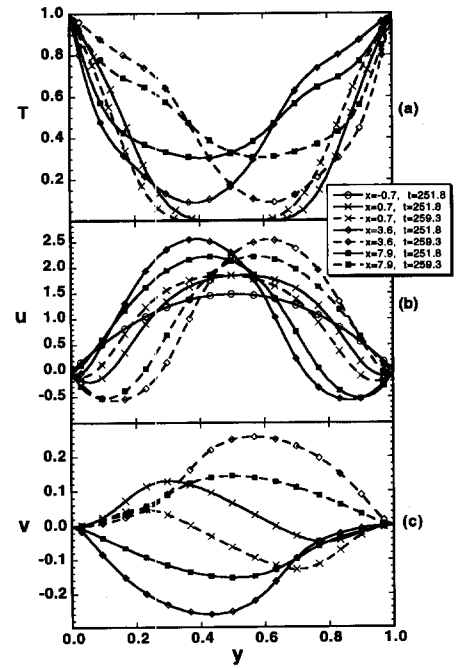


Fig. 5. Lateral variations of temperature (a) and velocity (b, c) at two times ($t = 251.8$ and 259.3) half a period apart; $Re = 219.7$, $Gr/Re^2 = 1.83$.

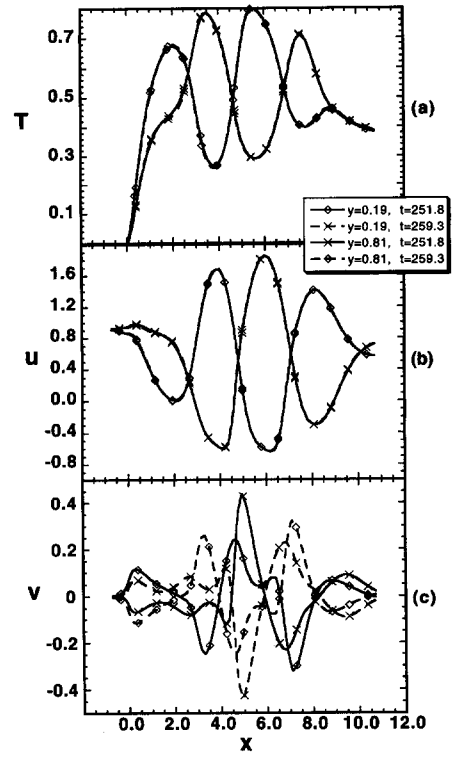


Fig. 6. Axial variations of temperature (a) and velocity (b, c) at two times ($t = 251.8$ and 259.3) half a period apart; $Re = 219.7$, $Gr/Re^2 = 1.83$.

the centerline half a period later; these reflections in time and space are also seen in Fig. 3.

The axial profiles of temperature and velocity along the channel centerline are shown in Fig. 7(a–c) at $t = 251.8$ and $t = 259.3$. In contrast to the stronger upward buoyant region near the wall where the flow is both upward ($u < 0$) and downward ($u > 0$) as shown in Fig. 6(b), $u$ at the centerline is always downward with alternating maxima and minima. At the centerline $T$ also has alternating maxima and minima; $v$ exhibits positive and negative values at the centerline as shown in Fig. 7(c) (also see Fig. 4c) and near the walls (Fig. 6c). Identical profiles of $T$ and $u$ occur half a period apart while the profile of $v$ is "opposite" half a period later.

The average Nusselt numbers shown in Fig. 8(a) show a periodic oscillation which exhibits a higher frequency component which is also present in the $v$ velocity component in Fig. 4(c). The time average of $Nu_{avg}$ is approximately 3.7. The local Nusselt numbers shown in Fig. 8(b) at $t = 251.8$ exhibit nonmonotonic variations.

The effects of increasing $Gr/Re^2$ for fixed $Re = 219.7$ are shown in Fig. 9 where the fields of $T$, $u$ and $v$ are shown for $Gr/Re^2 = 1.83$, 8.0 and 13.7. The three cases are shown at times when the temperature is a minimum at the location $x = 3.6$, $y = 0.19$. For increasing buoyancy there are stronger oscillations and a more pronounced effect near the start of the heated zone, $x = 0$. However, even for the large values of the mixed

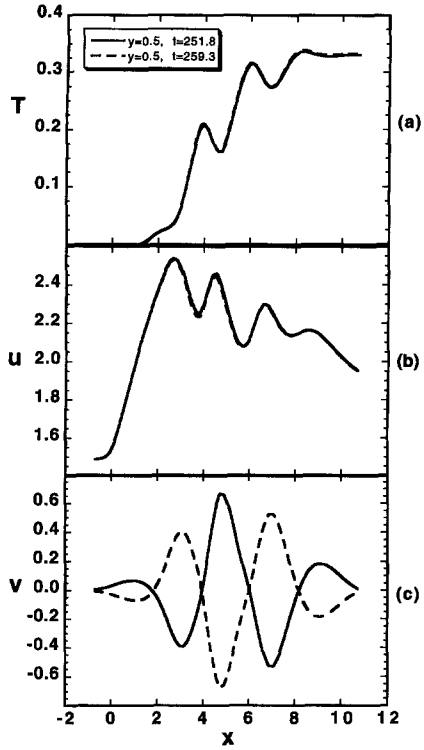


Fig. 7. Axial variation of temperature (a) and velocity (b, c) along the channel centerline at two times ($t = 251.8$ and 259.3) half a period apart; $Re = 219.7$, $Gr/Re^2 = 1.83$.

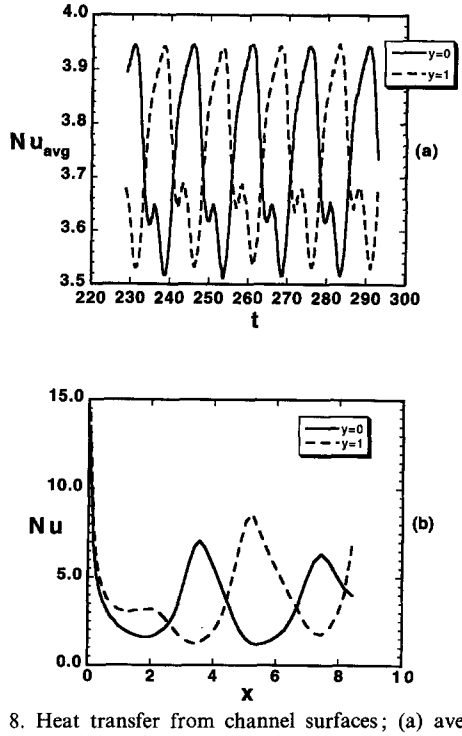


Fig. 8. Heat transfer from channel surfaces; (a) average Nusselt numbers; (b) local Nusselt numbers at $t = 251.8$; $Re = 219.7$, $Gr/Re^2 = 1.83$.

convection parameter there is little penetration of the heated, buoyant fluid upstream of the heated zone, $x < 0$ (for the cold isothermal boundary condition considered in this study where $T_s = T_{in}$ for $-4.3 \leqslant x < 0$).

The period of the oscillations decreases from 15.0 to 3.8 to 3.0 (frequency increases from 0.07, to 0.26 to 0.33) with increasing $Gr/Re^2$. The complexity and amplitudes of the oscillations has increased significantly from the simpler variations at lower buoyancy (Fig. 4) and are shown in Fig. 10 for the case $Gr/Re^2 = 13.7$. Note the increased amplitudes of $T$ and $v$ near the start of the heated region ($x = 0.7$). For this case, a spectral analysis of the temperature oscillations shows small components at two and three times the fundamental frequency of 0.33. Temperature oscillations with frequencies ranging from 0.003 to 0.1 in opposed flow mixed convection for different thermal boundary conditions [13], [17] and in tube flow [16] have been reported in the literature.

Lateral profiles similar to Fig. 5 were also obtained at the higher values of $Gr$ (not shown). These results show increased heating in the center of the channel and larger positive and negative values of both axial and lateral components of velocity, especially near the start of the heated region. Axial profiles of $T$, $u$ and $v$ near the walls at higher buoyancy ($Gr/Re^2 = 13.7$ in Fig. 11) show greater spatial variation and clearly exhibit the symmetric ($T$ and $u$) and antisymmetric ($v$) reflections that were previously noted for low buoyancy.

For increasing buoyancy ($Gr/Re^2 = 1.83$, 8.0, 13.7) the time average of $Nu_{avg}$ increases from 3.7 to 4.5 to 4.9, approximately; the $Gr/Re^2 = 13.7$ case is shown in Fig. 12 which also includes the local Nusselt number. There is an increased heat transfer near the start of the heated region (cf. Figs. 12(b) and 8(b)). We note that the above results for these time averaged Nusselt numbers are similar to those reported in other studies involving mixed convection; increasing heat transfer with increasing buoyancy has been observed although there is some evidence of a limited region of reduced heat transfer with increasing buoyancy in opposed mixed convection flow in converging channels with constant heat flux conditions [17].

## CONCLUSIONS

Unsteady, two-dimensional simulations of the downward flow of $N_2$ in a vertical heated (isothermal) channel with an upstream cold section show the importance of buoyancy. Results for the temperature, velocity and heat transfer have been obtained for $Re = 219.7$, $Pr = 0.7$ and $Gr/Re^2 = 1.83$, 8.0 and 13.7. To minimize property variations the temperature differences were small: i.e. 2, 8.7 and 15 degrees Kelvin for the three cases, respectively. For all cases there is an upward buoyant flow near the walls that turns downward at the top of the heated section. Near the walls, the axial flow reverses direction periodically;

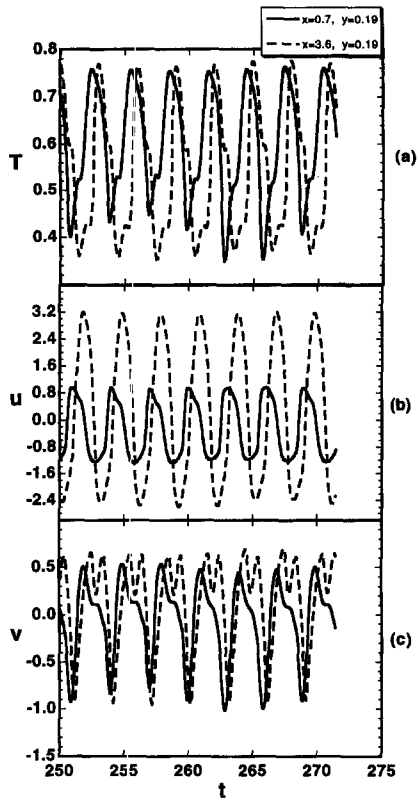


Fig. 10. Time variations of temperature (a) and velocity (b, c) at $y = 0.19$ and $x = 0.7, 3.6$; $Re = 219.7$, $Gr/Re^2 = 13.7$.

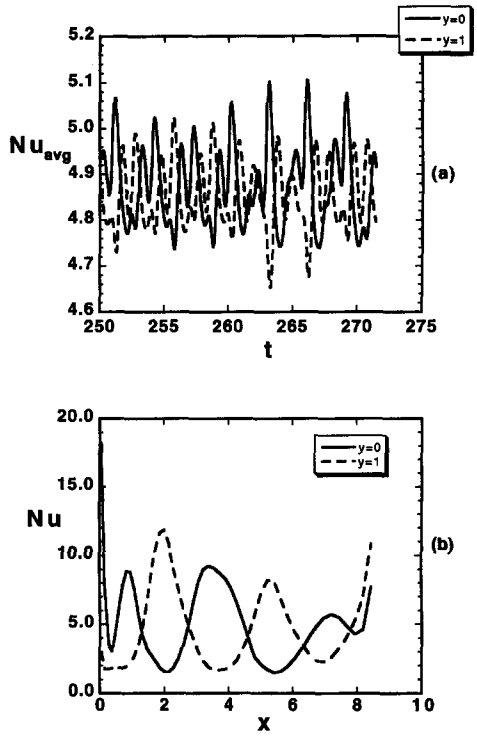


Fig. 12. Heat transfer from channel surfaces; (a) average Nusselt numbers; (b) local Nusselt numbers at $t = 260.4$; $Re = 219.7$, $Gr/Re^2 = 13.7$.

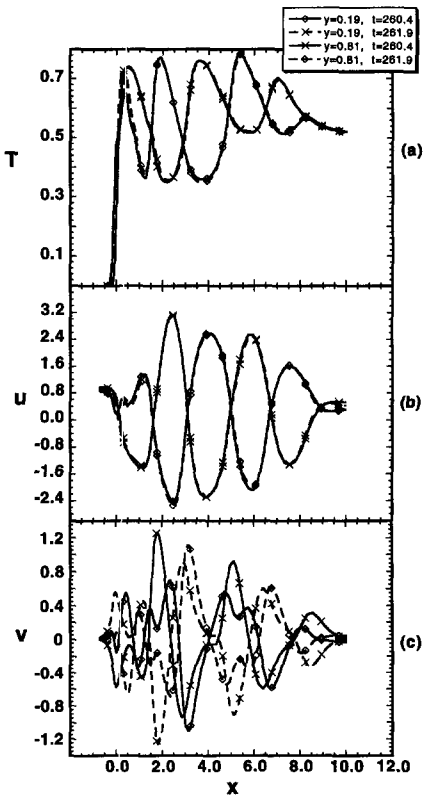


Fig. 11. Axial variations of temperature (a) and velocity (b, c) at two times ($t = 260.4$ and 261.9) half a period apart; $Re = 219.7$, $Gr/Re^2 = 13.7$.

the lateral flow reverses direction both at the centerline and near the walls. The temperature and axial component of velocity along the centerline of the channel are nonmonotonic and oscillatory. The results are nonsymmetric, periodic and exhibit increasing complexity and frequency for increasing buoyancy. The temperature and axial component of velocity half a period apart show symmetric reflections (of the asymmetric fields) while the lateral component of velocity, $v$, shows antisymmetric reflections. The average heat transfer is periodic and increases with increasing buoyancy.

*Acknowledgements*—the authors would like to thank Chris Shelton of the 3M company for sharing his data with us and for several valuable discussions. This work was supported by the U.S. Department of Defense (DARPA-DSO) Order no. 8951DPAM21264, and the U.S. Department of Energy, contract DE-AC04-94-AL85000. The DARPA monitor was William Barker.

## REFERENCES

1. Ostrach, S., Combined natural- and forced-convection laminar flow heat transfer of fluids with and without heat sources in channels with linearly varying wall temperatures, NACA TN 3141, 1954.
2. Morton, B. R., Laminar convection in uniformly heated vertical pipes. *Journal of Fluid Mechanics*, 1960, **8**, 227–240.
3. Scheele, G. F. and Hanratty, T. J., Effects of natural convection on stability of flow in a vertical pipe. *Journal of Fluid Mechanics*, 1962, **14**, 244–256.
4. Lawrence, W. T. and Chato, J. C., Heat-transfer effects

on the developing laminar flow inside vertical tubes. *Journal of Heat Transfer*, 1966, **88,** 214–222.
5. Zeldin, B. and Schmidt, F. W., Developing flow with combined free-forced convection in an isothermal vertical tube. *Journal of Heat Transfer*, 1972, **94,** 211–223.
6. Quintiere, J. and Mueller, W. K., An analysis of laminar free and forced convection between finite vertical parallel plates. *Journal of Heat Transfer*, 1973, **95,** 53–59.
7. Cebeci, T., Khattab, A. A. and LaMont, R., Combined natural and forced convection in vertical ducts. *Proceedings of 7th International Heat Transfer Conference*, Munich, Germany, 1982, Vol. 1, pp. 419–424.
8. Yao, L. S., Free and forced convection in the entry region of a heated vertical channel. *International Journal of Heat and Mass Transfer*, 1983, **26,** 65–72.
9. Shadday, Jr, M. A., Combined forced/free convection through vertical tubes at high Grashof numbers. *Proceedings of 8th International Heat Transfer Conference*, San Francisco, CA, 1986, Vol. 3, pp. 1433–1437.
10. Habchi, S. and Acharya, S., Laminar mixed convection in a symmetrically or asymmetrically heated vertical channel. *Numerical Heat Transfer*, 1986, **9,** 605–618.
11. Wang, M., Tsuji, T. and Nagano, Y., Mixed convection with flow reversal in the thermal entrance region of horizontal and vertical pipes. *International Journal of Heat and Mass Transfer*, 1994, **37,** 2305–2319.
12. Chang, T. S. and Lin, T. F., Steady and oscillatory opposing mixed convection in a symmetrically heated vertical channel with a low Prandtl number fluid. *International Journal of Heat and Mass Transfer*, 1993, **36,** 3783–3795.
13. Lin, T. F., Chang, T. S. and Chen, Y. F., Development of oscillatory asymmetric recirculating flow in transient laminar opposing mixed convection in a symmetrically heated vertical channel. *Journal of Heat Transfer*, 1993, **115,** 342–352.
14. Guerrero, H. N. and Hart, C. M., Flow instability and flow reversal in heated annular multichannels with initial downward flow. *Proceedings of the National Heat Transfer Conference*, 1993.
15. Rogers, B. B. and Yao, L. S., Finite-amplitude instability of mixed convection in a heated vertical pipe. *International Journal of Heat and Mass Transfer*, 1993, **36,** 2305–2315.
16. Joye, D. D. and Jacobs, S. W., Backflow in the inlet region of opposing mixed convection heat transfer in a vertical tube. *Proceedings of 10th International Heat Transfer Conference*, Brighton, 1994, Vol. 5, pp. 489–494.
17. Gau, C., Huang, T. M., and Aung, W., Mixed convection flow and heat transfer in a heated vertical convergent channel. Paper AIAA 94-2012, *6th AIAA/ASME Joint Thermophysics and Heat Transfer Conference*, Colorado Springs, CO, 1994.
18. Kee, R. J., Dixon-Lewis, G., Warnatz, J., Coltrin, M. E. and Miller, J. A., A Fortran computer code package for the evaluation of gas-phase multicomponent transport properties. *Sandia Report SAND*86-8246, 1986.
19. Kee, R. J., Rupley, F. M. and Miller, J. A., CHEMKIN-II : a Fortran chemical kinetics package for the analysis of gas-phase chemical kinetics. *Sandia Report SAND*89-8009, 1989.
20. Patankar, S. V., *Numerical Heat Transfer and Fluid Flow*. McGraw-Hill, New York, 1980.